Exploration of the NaxMoO2 phase diagram for low sodium contents ($x \leq 0.5$)

Laura Vitoux, Marie Guignard, Jacques Darriet, Claude Delmas

Exploration of the Na_xMoO_2 Phase Diagram for Low Sodium Contents ($x \leq 0.5$)

Laura Vitoux,[a] Marie Guignard,*[a] Jacques Darriet[a] and Claude Delmas[a]

The phase diagram of the layered Na_xMoO_2 system for low sodium contents ($x \leq 0.5$) was explored by electrochemical (de)intercalation in a sodium ion battery from the $Na_{2/3}MoO_2$ composition which is the only one obtained by solid state reaction at high temperature. This study was realized using electrochemistry combined with *in situ* X-ray diffraction for sodium contents x below 0.5. For the first time, four single phase domains ($x = 0.5$, $0.4 \leq x \leq 0.42$, $x = 0.37$, $x = 0.33$) were evidenced during the cycling of the Na_xMoO_2 based battery in the $0.25 \leq x \leq 0.5$ composition domain. All structural phase transitions are fully reversible. The existence of a superstructure was observed for the $Na_{0.5}MoO_2$ and $Na_{0.33}MoO_2$ compositions, attributed to the regular arrangements of both the sodium and molybdenum cations.

Introduction

While many of the sodium layered oxides $NaMO_2$ (M is a transition metal) were first discovered before the end of the 1960s,[1] layered oxides Na_xMO_2 with $x < 1$ were synthesized for the first time in the 1970s.[2] In the following decade these materials were studied for the first time as positive electrodes in Na batteries.[3] In the past ten years, they have been intensively studied again for their potential use as positive electrode materials in Na ion batteries.[4] In these materials, sodium electrochemical de-intercalation and intercalation can lead to structural rearrangements that affect the electronic properties of the layered oxides, and therefore their electrochemical performance. As shown the Na_xCoO_2 system, Na^+/Na^+ electrostatic repulsions between the $(MO_2)_n$ layers formed by edge-sharing MO_6 octahedra give rise to sodium ion/vacancy orderings and M^{3+}/M^{4+} charge ordering within these layers.[5]

Complex compositions with several transition metal ions have led to good electrochemical performances by limiting sodium ordering between the $(MO_2)_n$ layers, and therefore limiting the M^{3+}/M^{4+} charge ordering.[6] There is a fundamental interest in studying structural transitions in single-transition metal Na_xMO_2 systems, however, to gain understanding of the different mechanisms occurring in layered oxides upon cycling. Na_xMO_2 systems where M is a 3d element have already been intensively investigated from titanium to nickel.[3,7] For example, sodium/vacancy ordering has been found in most of the $Na_{1/2}MO_2$ phases where M is a 3d element,[8,9] whereas it has not been observed in $Na_{1/2}FeO_2$ nor in $Na_{1/2}TiO_2$ due to an irreversible Fe or Ti ion migration during the Na^+ deintercalation.[10] Moreover, it was observed that this sodium ion/vacancy ordering was correlated to the formation of V-V bonds in all the $Na_{1/2}VO_2$ polymorphs that were synthesized.[9]

Few studies report on sodium electrochemical (de)intercalation in Na_xMO_2 phases, where M is a 4d single element, used as positive electrode in a sodium battery.[11,12] Molybdenum system Na_xMoO_2 was first studied in 1984. Electrochemical and *in situ* X-ray powder diffraction studies performed on sodium batteries made with $Na_{2/3}MoO_2$ as the positive electrode revealed the complexity of the phase diagram MoO_2-Na_xMoO_2 .[11] Recently, we reinvestigated this system in the composition range $0.5 \leq x < 1$ to explain the multiple-step aspect of the electrochemical curve using *in situ* synchrotron X-ray powder diffraction during the charge and the discharge of a sodium battery made with $Na_{2/3}MoO_2$ as the positive electrode.[13] Thirteen single phase domains were evidenced in the composition range $0.5 \leq x < 1$,[13] whereas the previous study mentioned only five phases in the sodium content range $0.28 \leq x < 1$.[11]

Here we report the investigation of the Na_xMoO_2 phase diagram for sodium contents $x \leq 0.5$ using electrochemistry combined with *in situ* X-ray diffraction. We aim to understand the possible structural transitions occurring in this composition domain and provide evidence for the existence of specific Na_xMoO_2 compositions.

Experimental

The pristine material $Na_{2/3}MoO_2$ was synthesized by the solid state reaction reported in the literature.[11,14] Stoichiometric amounts of Na_2MoO_4 (from the dehydration of Na_2MoO_4, $2H_2O$ (Sigma-Aldrich, 99%)), Mo (VWR, 99,9%) and MoO_2 (Sigma Aldrich, 99%) were reacted in a gold tube sealed under argon for 90 hours at 700 °C after being previously ground together by ball milling (400 rpm/min for 3h). The product, a well crystallized black powder, was recovered in a glovebox under argon atmosphere. Small amounts of Na_2MoO_4 and Mo were present as impurities. These result from the decomposition of the layered Na_xMoO_2 phase at high temperature and their presence implies a deficit of sodium in the pristine material. The chemical composition was re-evaluated to $Na_{0.63}MoO_2$ according to the initial voltage measured when the material was used as a positive electrode in a sodium ion battery.[13]

Electrochemical studies were carried out on Na | $NaPF_6$ + 2% FEC in PC (1M) | Na_xMoO_2 batteries assembled in airtight 2032 type coin cells. At the positive electrode, the active material was mixed with carbon black to improve its electronic conduction and with PTFE (polytetrafluoroethylene) used as binder in a 88:10:2 weight ratio. Sodium batteries were galvanostatically charged and discharged at C/100 rate (1 Na^+ per formula unit (de)intercalated in 100 h) between 1.7 V and 3.5 V. The de-intercalated Na_xMoO_2 phases were obtained by potentiostatic synthesis performed in a Swagelok-type sodium battery, with a pellet of $Na_{2/3}MoO_2$ mixed with carbon black (90:10 in weight)

used as the positive electrode. The batteries were first charged galvanostatically to the voltage corresponding to the Fermi level of the targeted composition (2.5 V for $Na_{0.5}MoO_2$ and 3.5 V for $Na_{\sim 0.3}MoO_2$ vs Na^+/Na) and this voltage was continuously applied during the potentiostatic step until the current reached zero. The resulting materials were then recovered in a glovebox under argon, washed with dimethyl carbonate and dried under vacuum in order to be characterized by powder X-ray diffraction.

Laboratory based X-ray powder diffraction measurements (Cu-source Panalytical X'Pert Pro) were performed on $Na_{\sim 0.3}MoO_2$ loaded in sealed glass capillaries (0.2 mm diameter). High resolution X-ray powder diffraction data for $Na_{0.5}MoO_2$ loaded in a sealed kapton capillary (0.8 mm diameter) were collected at 11-BM beamline at the Advanced Photon Source (APS) at Argonne National Laboratory using an average wavelength of 0.41417(2) Å. Discrete detectors covering an angular range from -6 to 16 ° were scanned over a 34 ° 2θ-range, with data points collected every 0.001 ° and scan speed of 0.01°/s. The powder was loaded in a sealed 0.8 mm diameter capillary. High resolution X-ray diffraction measurements were also performed at this beamline, using an average wavelength of 0.414224 (2) Å, at different temperatures: 100 K, 200 K, 260 K, 295 K, 380 K et 473 K. Le Bail refinements were carried out using the JANA2006 program.[15]

Pair distribution functions (PDFs) were calculated for $Na_{0.5}MoO_2$ (the same sample as the one used for high resolution X-ray powder diffraction) from powder diffraction data recorded at 11-ID-B beamline at the APS using a wavelength of 0.2114 Å. The diffraction data recorded on an empty kapton capillary in the same conditions have been used to correct the diffracted intensity from the background. The measured diffracted intensity has been corrected from the incoherent scattering, the background, the polarization and the absorption using the ad-hoc method provided by PDFgetX3 software.[16] The corrected intensity I(Q) and the structure function S(Q) have been calculated using this program, with $Q = 4\pi\sin\theta/\lambda$. Reduced PDFs G(r) have been obtained by Fourier transforming S(Q) functions over the 0.5-24 $Å^{-1}$ Q-range. Calculated PDFs have been obtained using the PDFgui software.[17]

An *in situ* powder X-ray diffraction experiment was performed using a laboratory based X-ray powder diffractometer during the electrochemical process (Panalytical Empyrean diffractometer operating with Cu $K\alpha_1$ radiation). An electrochemical cell specifically designed to enable X-ray diffraction acquisitions through a beryllium window was used. After a first galvanostatic charge to 2.5 V (which corresponds to a sodium electrochemical de-intercalation until the chemical composition of the positive electrode reaches $Na_{0.5}MoO_2$), the battery was charged using the Galvanostatic Intermittent Titration Technique (GITT) to 3.8 V ($Na_{\sim 0.25}MoO_2$) alternating 1 hour of charge at C/100 and 4 hours of relaxation period. The cell was then discharged under the same conditions back to 2.5 V. X-ray diffraction data were collected for 2 hours at the end of each relaxation period over the 2θ-range $13° \leq 2\theta \leq 46°$. Le Bail refinements were carried out using the JANA2006 program.[15]

Results

Electrochemical characterization

The starting material $Na_{2/3}MoO_2$ was obtained from solid state synthesis and used as a positive electrode in a sodium ion battery. The battery was cycled between 1.7 V ($Na_{\sim 0.63}MoO_2$) and 3.5 V ($Na_{\sim 0.28}MoO_2$) at a low rate (C/100). The first cycles are presented **Figure 1** along with the resulting derivative curve dE/dx = f(x). Electrochemical sodium (de)intercalation is shown to be reversible in this voltage range, in agreement with the previous electrochemical study of this system.[11] However, a slight shift towards lower sodium contents is observed for the second charge. This is due to the degradation of the liquid electrolyte $NaPF_6$ in PC (1M) + 2 % FEC at high voltage which induces an imprecision on the calculation of the sodium contents that are therefore evaluated only on the first charge (derivative) curve. Although this liquid electrolyte was found to be stable in the 0-5 V window voltage range when aluminum was used as the working electrode,[18] we empirically observed that the electrochemical stability of liquid electrolytes actually depends on the nature of the transition metal ion present in the layered oxide used as the positive electrode.

The first charge of the battery begins with a multi-step variation of the cell voltage in the $0.5 \leq x \leq 0.63$ composition domain. It results from the existence of several narrow single phase domains close in sodium content. This was previously reported in our first investigation of the Na_xMoO_2 system for high sodium contents ($x \geq 0.5$) by *in situ* X-ray diffraction.[13] For x = 0.5 a large voltage step (0.9 V) is observed, indicating the formation of a very stable phase. A detailed study of the material in the vicinity of this composition is presented in the next section.

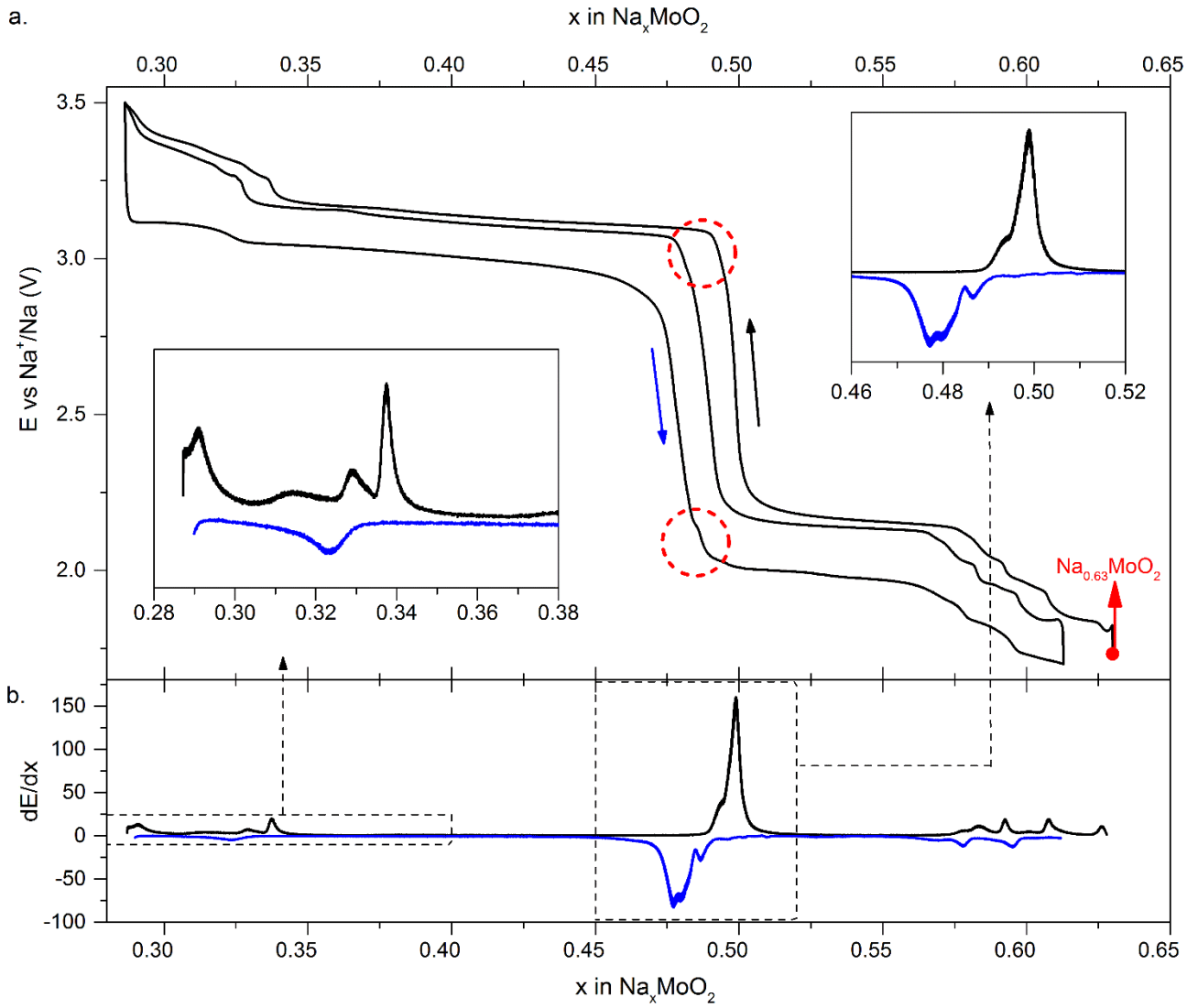

Figure 1: (a) First galvanostatic cycle of the electrochemical cell made with $Na_{2/3}MoO_2$ as the positive electrode. (b) dE/dx derivative curves recorded on charge (black) and discharge (blue).

For sodium content x < 0.5, the variation of the cell voltage is less complex, suggesting a simple phase diagram. Firstly, the voltage continuously increases until the $Na_{0.37}MoO_2$ composition, suggesting the existence of a solid solution in the $0.37 \leq x \leq 0.5$ composition range.

A biphasic domain between $Na_{\sim 0.37}MoO_2$ and $Na_{0.33}MoO_2$ is then indicated by a voltage plateau around 3.17 V. Several small voltage steps occur in the x-range $0.30 \leq x \leq 0.34$. This is particularly visible on the section of the dE/dx charge derivative curve (presented in the insert in Figure 1) where two peaks characteristic of Na_xMoO_2 single phases appear at $x \approx 0.34$ as well as $x \approx 0.33$. No strict conclusions can be made regarding the phase transitions observed at x < 0.33 on the charge curve because they may result from the electrolyte degradation observed even at this moderate voltage. On discharge, these transitions are less visible on the electrochemical curve. It should be noted that the compositions derived from the discharge curve are slightly shifted to lower values due to polarization phenomena. This type of behavior is observed when the formation energy of a new phase is different to that required to make the opposite reaction. However, the features of the second charge are very similar to those of the first charge, implying that the previously described transitions are completely reversible.

Structural characterization of the $Na_{0.5}MoO_2$ material

As a large voltage step is observed around the $Na_{0.5}MoO_2$ composition, a sodium ordering was thought to exist at this composition that would explain the relative stability of this phase. High resolution X-ray powder diffraction was therefore used to try to determine the structure of the material $Na_{0.5}MoO_2$ obtained by potentiostatic sodium electrochemical de-intercalation. Its pattern is shown in Figure 2.

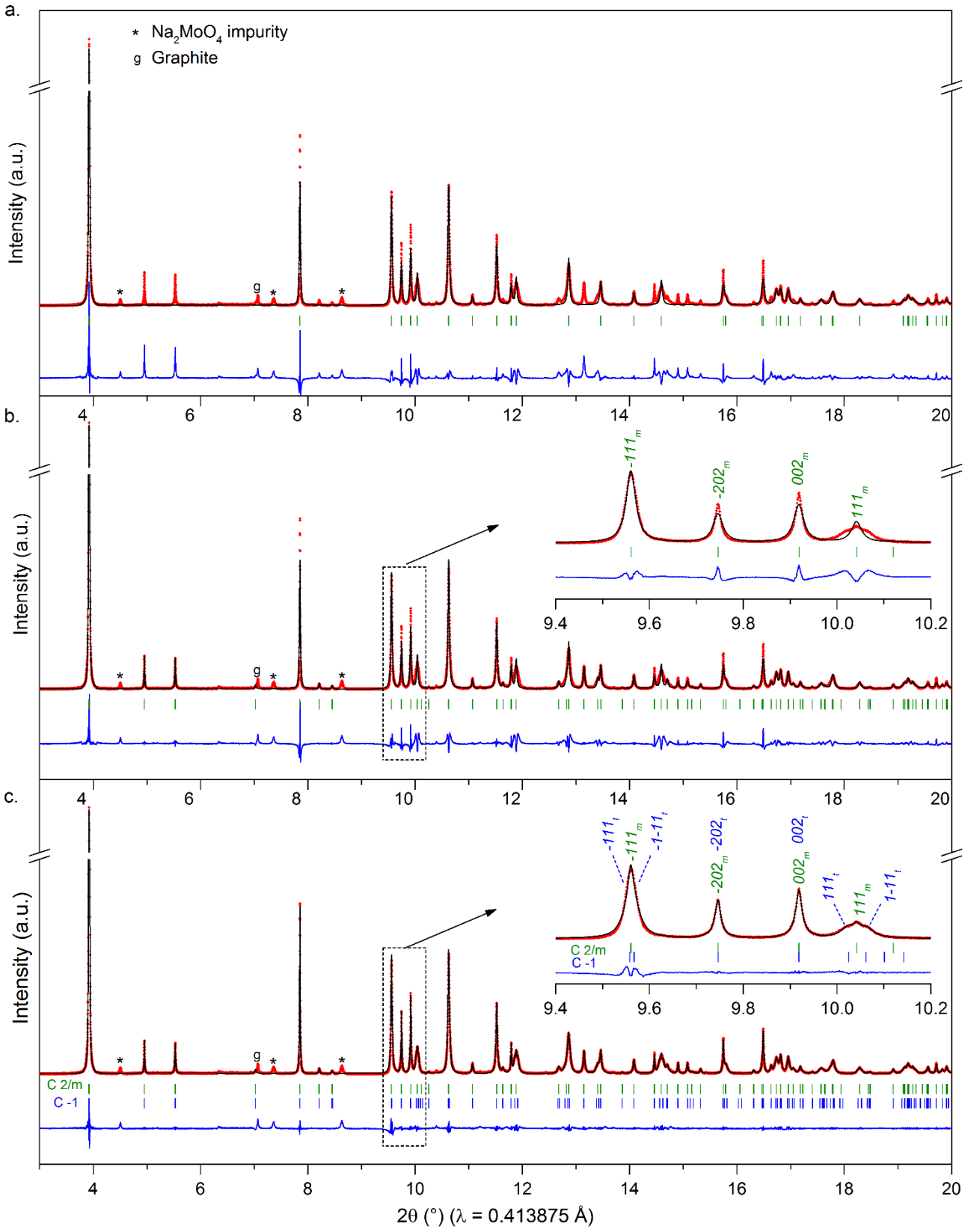

Figure 2: Experimental high resolution X-ray powder diffraction pattern of $Na_{0.5}MoO_2$ (red diamonds), calculated pattern obtained from the Le Bail refinement (black line) considering the O'3 monoclinic subcell (a), the monoclinic supercell (b) and a mixture of monoclinic and triclinic supercells (c). Enlargements are also shown for (b) and (c) in the inset (top right). The difference lines are shown in blue and vertical bars show the position of the Bragg reflections.

At first, we found that the diagram could be indexed using the monoclinic cell (Space group: C2/m) proposed for a similar layered molybdenum oxide, $NaMo_2O_4$.[19] In this structural model, sodium ions were not found to be ordered and it was proposed that they partially occupied all the available octahedral interstitial sites. However, it was shown that molybdenum atoms were shifted from the center of their octahedral sites within the $(MoO_2)_n$ layers to form infinite zigzag chains with short Mo-Mo distances within the chains (2.535 Å) and long Mo-Mo inter-chains distances (3.20 Å). This cell corresponds to a superstructure (Number formula units Z = 4) of the classical subcell (Z = 2, space group: C2/m, noted as the O'3 subcell) usually used to describe the structure of sodium layered oxides when a monoclinic distortion of the O3 hexagonal symmetry occurs.

The refined cell parameters for our sample were found to be only slightly different compared to those reported previously.[19] The profile refinement performed using Le Bail method considering both the subcell and superstructure cell is shown in Fig. 2 a and b, respectively, along with the experimental data. The refinement considering the superstructure gives the following cell parameters: a = 12.454(1) Å, b = 2.8861(2) Å, c = 4.9332(3) Å, β = 103.969(6)°. The indexation of two diffraction reflections around 5° is only possible when the supercell is used, indicating the existence of a superstructure for $Na_{0.5}MoO_2$. However, for *hkl* reflections with $k \neq 0$, shoulders on both sides of the diffraction peaks were observed and could not be indexed using this monoclinic cell. (**Insert Figure 2b and Figure S1**). This suggests that a second phase with a very similar layered structure but with a triclinic symmetry coexists, leading to the splitting of the *hkl* reflection into two reflections, *hkl* and *h-kl*. The cell parameters of the secondary phase with the triclinic symmetry are deduced from those of the monoclinic cell: α and γ were allowed to deviate from 90 °. A profile refinement was performed using Le Bail method and a good fit of the experimental data was achieved considering two phases (Figure 2c). To make the comparison of the cell parameters of each phase possible, a non-standard space group C-1 was used for the triclinic phase to refine its cell parameters. They were found to be very close to those of the monoclinic phase: a = 12.455(1) Å, b = 2.8854(2) Å, c = 4.9334(1) Å, α = 89.90(1)°, β = 103.96(1)°, γ = 89.79(1)°.

A close look on the electrochemical curve around $Na_{0.5}MoO_2$ composition reveals a change in slope at the top and at the bottom of the voltage step in charge and in discharge, respectively (encircled in red dashed lines on **Figure 1a**). Moreover, several peaks are observed for the same composition range on the derivative curve dE/dx = f(x) (**Insert in Figure 1a**). In order to have more insight on this peculiar behavior a cyclic voltammetry experiment was performed between 2.0 V and 3.1 V at 6µ V/s corresponding to an average C/500 rate (**Figure S2**). The presence of several reversible peaks alongside the main redox process, which remain after 3 cycles, shows the complexity of the electrochemical de-intercalation and intercalation at the $Na_{0.5}MoO_2$ composition. This shows that several single phases Na_xMoO_2 exist with a composition close to $Na_{0.5}MoO_2$, including those with the monoclinic and the triclinic symmetries. Collecting X-ray diffraction patterns at various voltages between 2.1 V and 3.0 V during *in situ* experiments did not allow isolating neither the monoclinic phase nor triclinic one. In all cases diffraction peaks characteristic of both materials were always simultaneously observed.

A thermal treatment was then used to try to isolate one of the two phases existing with a composition close to $Na_{0.5}MoO_2$. Increasing the temperature would indeed favor the existence of the phase with the most symmetric structure (here monoclinic) whereas lowering it would allow to isolate the less symmetric structure (here triclinic). High-resolution powder X-ray diffraction patterns of the $Na_{0.5}MoO_2$ material were therefore collected at various temperatures when the sample was heated up (100 K, 200 K, 260 K, 295 K, 380 K and 473 K) (**Figure 3a**). No significant change was observed on the X-ray diffraction patterns during the heat treatment, indicating that the layered structure was stable over this temperature range. To follow the evolution of the monoclinic phase/ triclinic phase ratio, the X-ray diffraction patterns in the 2θ-range 9.4° - 10.2° are shown in **Figure 3b**. The evolution in the proportion of the triclinic phase is highlighted by the changes in intensity of the -111_t and $-1-11_t$ reflections at approximately 9.56°, as well as that of 111_t and $1-11_t$ ones at approximately 10.04°. The intensity of these reflections decreases at high temperature and increases at low temperature, indicating that, as expected, the triclinic phase is stabilized at low temperature and the monoclinic phase at high temperature. However, none of these two phases were isolated in this temperature range which was limited by the experimental setup. The presence of two phases whose structures have very close cell parameters leads to an important overlapping of the Bragg reflections. No reliable structural model could therefore be determined from powder X-ray diffraction data.

Experimental reduced PDFs were obtained at room temperature for the same sample $Na_{0.5}MoO_2$ which was used for the high-resolution powder X-ray diffraction data collection (**Figure 4**). As the sample contains two phases, it was not possible to determine any structures from the experimental reduced PDFs. Nevertheless, they clearly show that the molybdenum atoms rearrange within the $(MoO_2)_n$ layers to form short Mo-Mo bonds (2.53 Å), intermediate Mo-Mo bonds (2.88 Å) and long Mo-Mo bonds (3.20 Å). These experimental Mo-Mo distances are compatible with those in the Mo-Mo zig-zag chains that were found in $NaMo_2O_4$ from single crystal diffraction.[19]

The presence of the two phases with a composition close to $Na_{0.5}MoO_2$ was always observed after the sodium electrochemical de-intercalation from several batches of $Na_{2/3}MoO_2$. One can assume that two phases are already present in the initial material $Na_{2/3}MoO_2$, resulting from a small inhomogeneity in composition for example, and that their structure will only be different for a composition close to $Na_{0.5}MoO_2$. A similar behavior was observed for $LiCoO_2$, which can exist with a small lithium excess (lithium ions occupy cobalt sites and oxygen vacancies ensure the electroneutrality).

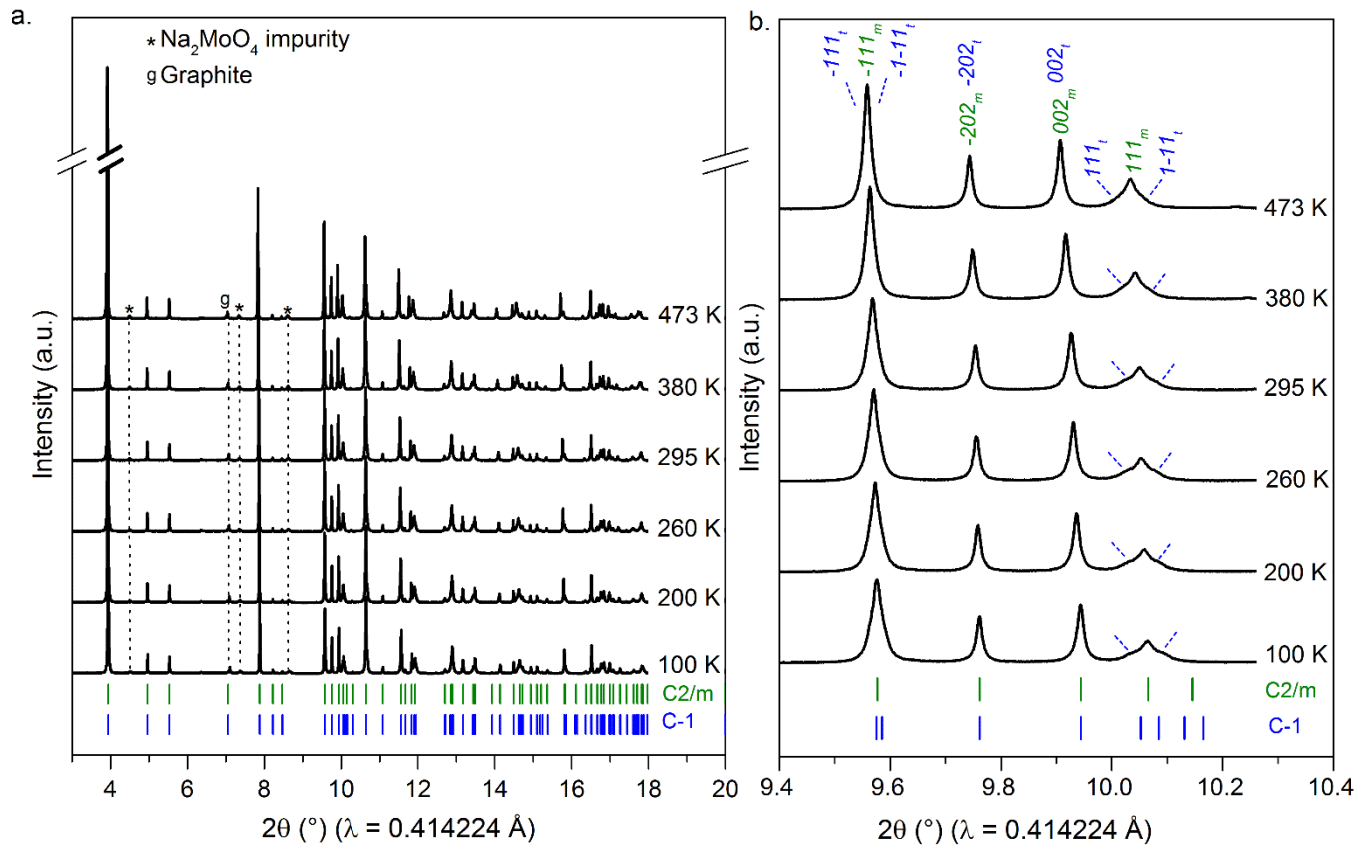

Figure 3: Experimental high resolution X-ray powder diffraction pattern of $Na_{0.5}MoO_2$ recorded at different temperature. Vertical bars show the position of the Bragg reflections.

When lithium is de-intercalated to reach the composition $Li_{0.5}CoO_2$, two phases coexist. One is obtained from the stoichiometric $LiCoO_2$ whose structure is monoclinic, whereas the other one comes from the Li over-stoichiometric "$LiCoO_2$" whose structure remains hexagonal.[20] Both materials coexist in the real samples used in commercial batteries.

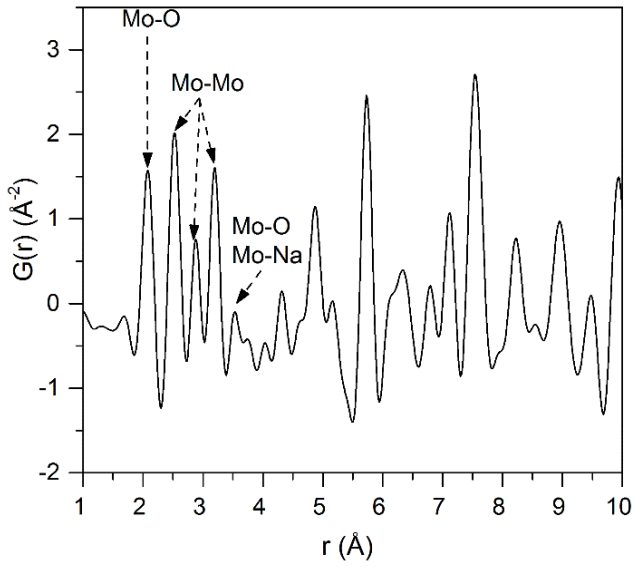

Figure 4: Experimental reduced pair distribution functions (PDFs), G(r), of $Na_{0.5}MoO_2$

***In situ* X-ray diffraction**

General overview

To better understand the structural transitions occurring during the electrochemical process in the Na_xMoO_2 material for $x \leq 1/2$, an *in situ* X-ray diffraction experiment was performed during the charge and the discharge of the battery made of $Na_{2/3}MoO_2$ at the positive electrode. The cell was cycled in the 2.5 V – 3 V range. Prior to the experiment, the cell is charged to 2.5 V to reach $Na_{0.5}MoO_2$ composition. All X-ray diffraction patterns collected during the experiment are represented next to the electrochemical GITT curve (**Figure 5**). The general evolution of the X-ray diffraction patterns shows the good reversibility of the de-intercalation process.

To establish the phase diagram, X-ray diffraction patterns are enlarged in three 2θ-ranges and represented along with the electrochemical curve to compare the structural transitions to the voltage changes (**Figure 6**). In discharge the general evolution is very similar to that observed during the charge. Nevertheless, in the 0.37 – 0.50 range, the diffraction peaks are broader than those observed in charge. This is an evidence of a hysteresis phenomenon due to the nucleation mechanism, which will be further discussed. However, at the very end of the re-intercalation the $Na_{0.5}MoO_2$ phase is still obtained with a diffraction pattern very similar to that of the initial material. The comparison of the X-ray diffraction patterns emphasizes the reversibility of the structural transitions.

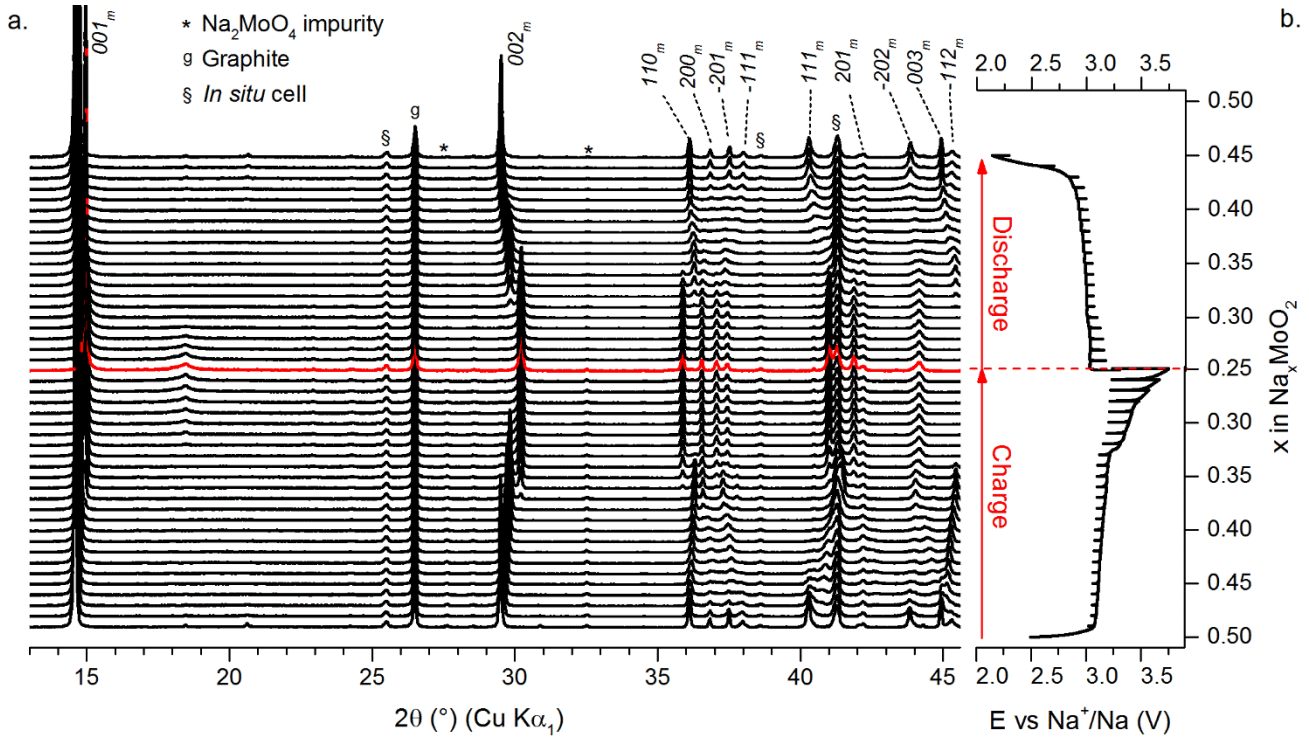

Figure 5: X-ray powder diffraction patterns collected during the *in situ* experiment. Indexation of the $Na_{0.5}MoO_2$ composition (top patterns) is giving in the O'3 monoclinic subcell. (b) Electrochemical curve recorded in GITT mode during the *in situ* experiment.

Determination of the phase diagram from the *in situ* X-ray diffraction study upon charge

Due to the instability of the electrolyte above 3.3 V, which is magnified in the low rate GITT experiment, the phase diagram was studied during the charge (**Figure 6a**). The discharge shows only the reversibility of the process. All the experimental X-ray diffraction patterns recorded during the *in situ* experiment were found to have similarities with that of $Na_{0.50}MO_2$. In the previous part we have shown the existence of a superstructure (Z = 4) for this composition characterized by two diffraction reflections in the 2θ-range 5-6° that can only be indexed using the superstructure cell. These diffraction peaks are visible on in the 2θ-range 18-21 ° on the X-ray diffraction patterned during the *in situ* experiment performed in our laboratory. As soon as sodium is de-intercalated from the $Na_{0.5}MoO_2$ phase, they disappear; they reappear in discharge for the composition $Na_{0.5}MoO_2$

The common monoclinic subcell with Z = 2 was therefore used to index the most intense reflections on its X-ray diffraction pattern recorded during the *in situ* experiment to facilitate comparisons with the different phases obtained during the electrochemical process. Cell parameters of these phases are reported **Table 1.** The evolution of the position of the 002_m reflection is correlated to the distance between two successive $(MoO_2)_n$ layers and it is a good indicator to differentiate solid solutions from biphasic domains.[13,21] The overall changes in the cell parameters are emphasized by the displacement of the 110_m, -201_m, -111_m and 200_m reflections.

As sodium is de-intercalated from $Na_{0.5}MoO_2$, X-ray diffraction peaks at high angles broaden until $Na_{0.37}MoO_2$ is formed. The phase diagram is therefore deduced only from the evolution of the 002_m diffraction peak in the $0.37 \leq x \leq 0.5$ composition domain. From $Na_{0.42}MoO_2$ composition, the 002_m reflection continuously shifts towards higher angles with no change in its width until $Na_{0.4}MoO_2$ is obtained. This is characteristic of a solid solution behavior. At high angles, some diffraction peaks are still very broad suggesting that structural defects exist in the layered structure in this composition domain.

Table 1: Refined cell parameters for specific Na_xMoO_2 phases obtained from the profile refinement performed using the Le Bail method with X-ray diffraction data collected during the charge of the *in situ* experiment.

x in Na_xMoO_2	Space group	Cell parameters				Interslab distance (Å)
		a (Å)	b(Å)	c (Å)	β (°)	
0.50	C2/m	4.9318(8)	2.8852(4)	6.1165(7)	99.03(1)	6.041
0.37	C2/m	4.949(1)	2.8906(8)	6.2141(5)	105.90(1)	5.976
0.33	C2/m	4.963(1)	2.9264(6)	6.1085(9)	105.04(2)	5.899

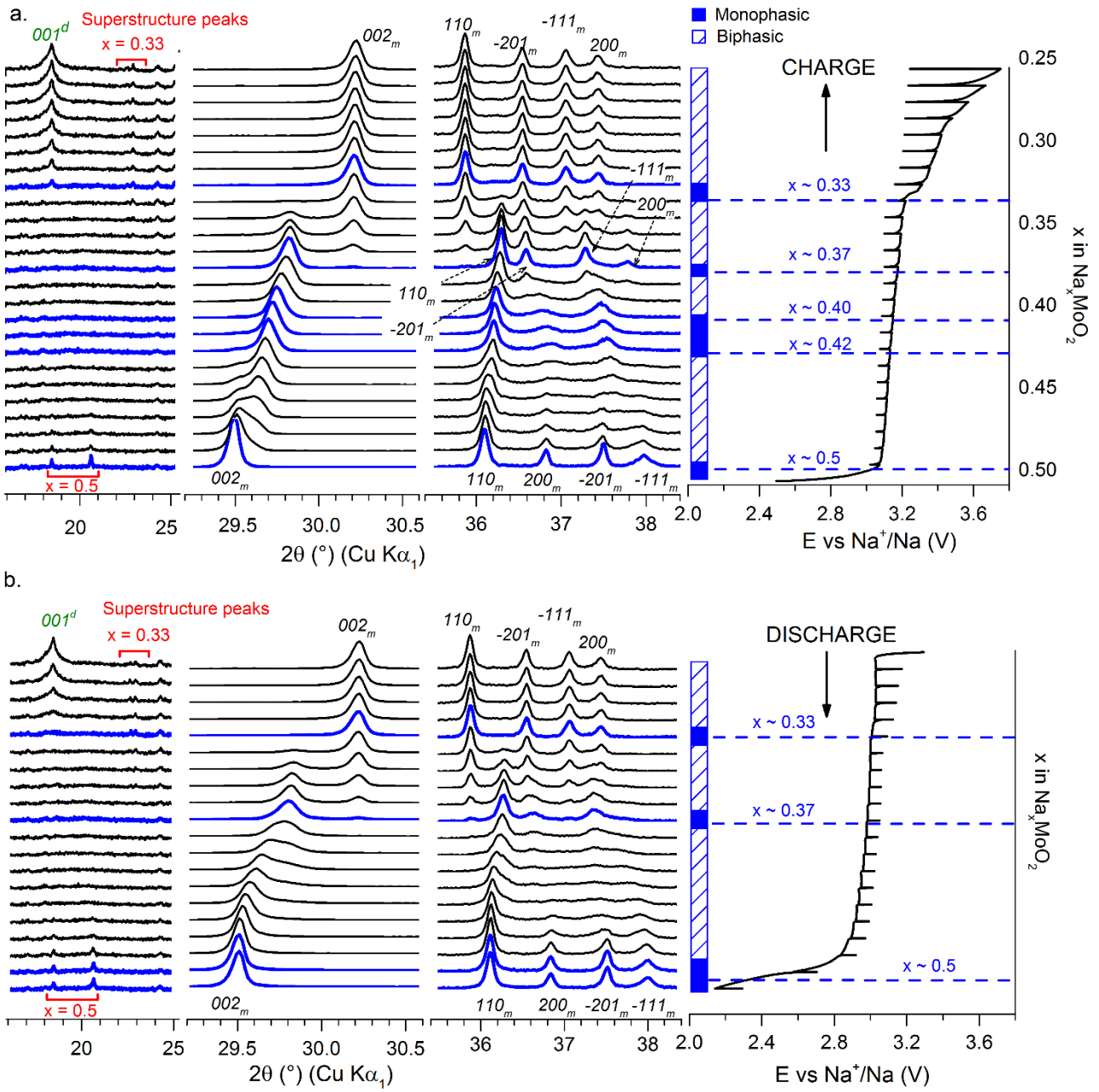

Figure 6: Zoom over X-ray diffraction patterns collected during the *in situ* experiment in the 0.25 ≤ x ≤ 0.5 composition range during (a) charge and (b) discharge.

Between $Na_{0.4}MoO_2$ and $Na_{0.37}MoO_2$ compositions the 002_m diffraction peak broadens and narrows again, indicating the existence of a new biphasic domain which was not suggested by the electrochemical characterization. For $Na_{0.37}MoO_2$, diffraction peaks at high angles become narrow again indicating a better homogeneity for this composition. When sodium is de-intercalated from $Na_{0.37}MoO_2$ a biphasic domain occurs between $Na_{0.37}MoO_2$ and $Na_{0.33}MoO_2$ compositions with a significant shift of the 002_m diffraction peak towards higher angles. This indicates a sharp decrease of the interlayer distance for $Na_{0.33}MoO_2$.

The formation of the $Na_{0.33}MoO_2$ phase is associated to the voltage step observed on the electrochemical curve at 3.3 V. Moreover, the X-ray diffraction pattern of $Na_{0.33}MoO_2$ shows extra diffraction peaks at small angle at approximately 23°, which are not indexed in the monoclinic subcell (Z = 2, space group: C2/m). These peaks could be the result of sodium/vacancy orderings between the $(MoO_2)_n$ slabs, which would particularly be expected for this sodium content (x = 1/3).[22] As it was discussed for Na_xMoO_2 phases with sodium contents x > 0.5,[13] Mo-Mo bonds patterning in the $(MoO_2)_n$ slabs could also be expected which could affect the transport properties within the positive electrode material upon cycling.

After the voltage step, there is no variation of the X-ray diffraction pattern of the $Na_{0.33}MoO_2$ phase. Nevertheless, a broad diffraction peak appears at 18.6° (d = 4.77 Å). Given its position, width and constant increasing intensity upon sodium de-intercalation, this peak is likely correspond to the *00l* reflection of a highly de-intercalated phase Na_tMoO_2 with a very short interlayer distance.

Such highly de-intercalated phases have been evidenced in several other Na_xMO_2 systems. For example, in P2-

$Na_xMn_{1/2}Fe_{1/2}O_2$ and O3-$Na_xMn_{1/3}Fe_{2/3}O_2$,[23] broad diffraction peaks appeared at high voltage and they were thought to belong to a highly de-intercalated, poorly crystallized phase (x ≈ 0.15). In P2-$Na_x(Ni_{1/3}Mn_{2/3})O_2$[24] and O3-$Li_xMO_2$ (M = Ni, Co)[25-27], the alkali de-intercalation is complete and leads respectively to the formation of O2-$(Ni_{1/3}Mn_{2/3})O_2$, O1-NiO_2 and O1-CoO_2 phases. The interlayer distances measured in O1-CoO_2 (4.29 Å[27]) and O1-NiO_2 (4.52 Å[26] , 4.34 Å[28]) are in the same order of magnitude as the interplanar distance measured from the *in situ* X-ray diffraction patterns (4.77 Å).

Nevertheless, the relative intensity of the *00l* reflection is very low compared to the *001* peak of the $Na_{0.33}MoO_2$ phase, even on the last X-ray diffraction pattern collected at high voltage during the *in situ* experiment. Attempts to continue the charge beyond 3.8 V in order to increase the relative intensity of the *00l* reflection and observe additional diffraction peaks belonging to Na_tMoO_2 were unsuccessful. At this voltage, there is a strong polarization and a degradation of the liquid electrolyte occurs that prevents further sodium de-intercalation from $Na_{0.33}MoO_2$. Therefore we cannot determine precisely the structure nor the composition of this highly de-intercalated phase.

X-ray diffraction patterns were also collected during the discharge of the electrochemical cell back to 2.5 V corresponding to the $Na_{0.5}MoO_2$ composition (**Figure 6b**). Firstly re-intercalation of sodium into the Na_xMoO_2 material at high voltage induces the disappearance of the *00l* diffraction peak of the highly de-intercalated phase Na_tMoO_2. This shows that the sodium de-intercalation is reversible and the intercalation within the highly de-intercalated phase is possible. This confirms that this latter phase still has a layered structure. As previously suggested by the aspect of the electrochemical discharge curve (**Figure 1**), the behavior of the Na_xMoO_2 material during the discharge of the cell (**Figure 6b**) is slightly different for x > 0.33 than the one previously described during the charge (**Figure 6a**). After sodium intercalation into $Na_{0.33}MoO_2$, two successive biphasic domains occur. Their existence is indicated by the continuous shifting and broadening of the *002* reflection in both single phase domains. No well crystallized single phase is observed for the composition $Na_{0.37}MoO_2$ nor solid solution in the composition range 0.4 ≤ x ≤ 0.42. However, the broadening of the diffraction reflections induced by the strong structural rearrangement occurring prior to the formation of $Na_{0.5}MoO_2$ phase is still observed during the discharge.

Discussion

$(MoO_2)_n$ stacking

To complete the phase diagram, the stacking types adopted by the structure of the Na_xMoO_2 phases (x < 0.5) were determined. Reliable structural determination could not be achieved using the Rietveld method on the X-ray diffraction patterns collected during the *in situ* experiment due to the limited number of reflections recorded during this experiment.

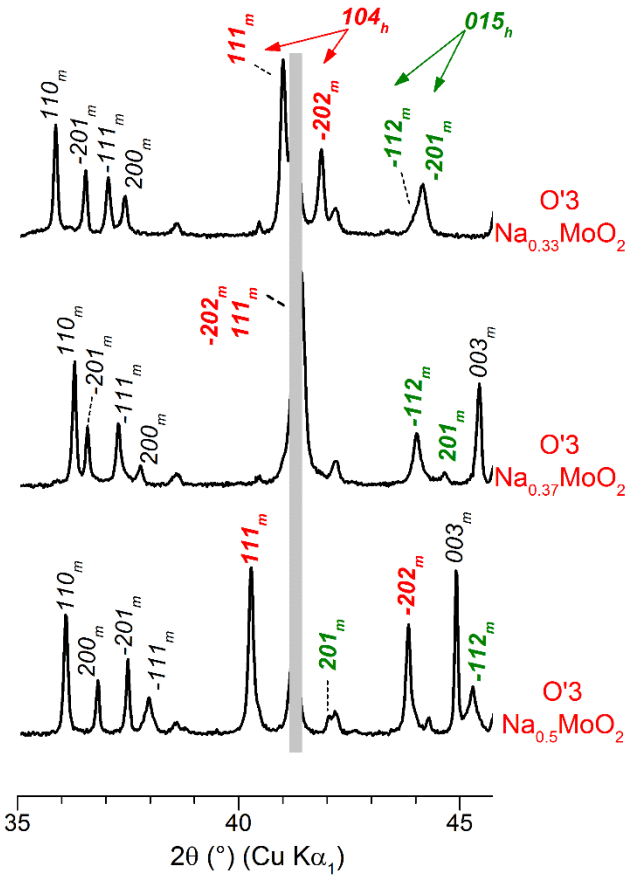

Figure 7: Determination of the stacking type of the structure of the main single phases based on the intensity ratio of reflections issued from 104_h and 015_h. Diffraction peaks from the *in situ* cell were hidden by gray rectangles.

However information regarding the stacking of the $(MoO_2)_n$ layers and the geometry of the interstitial sites occupied by sodium can be empirically determined by analyzing the intensity ratio of two sets of two Bragg reflections.[13] When 111_m and -202_m reflections, arising from the splitting of the 104_h reflection in the hexagonal cell due to the monoclinic distortion, are more intense than -112_m and 201_m ones, arising from the splitting of the 015_h reflection in the hexagonal cell, it indicates that sodium ions occupy octahedral sites, whereas they occupy trigonal prismatic sites when -112_m and 201_m reflections are more intense. The intensity ratio between these two sets of reflections was studied using the X-ray diffraction patterns collected during the charge. The zoom of the X-ray patterns of three main Na_xMoO_2 single phases obtained in this study (x = 0.5, 0.37 and 0.33) in the relevant 2θ-range is presented **Figure 7**. It reveals clearly that sodium occupies octahedral sites in $Na_{0.5}MoO_2$ and $Na_{0.33}MoO_2$ as 111_m and -202_m reflections are more intense. Unfortunately, these reflections are hidden for $Na_{0.37}MoO_2$ by a sharp diffraction peak coming from the *in situ* cell. However, sodium ions seem to be located in octahedral sites too in this material as the intensity of the -112_m and 201_m reflections is low. This indicates that sodium environment does not evolve during the sodium electrochemical de-intercalation and intercalation in Na_xMoO_2 phases in the composition range x ≤ 0.5 and that these phases all have the O'3-type structure.

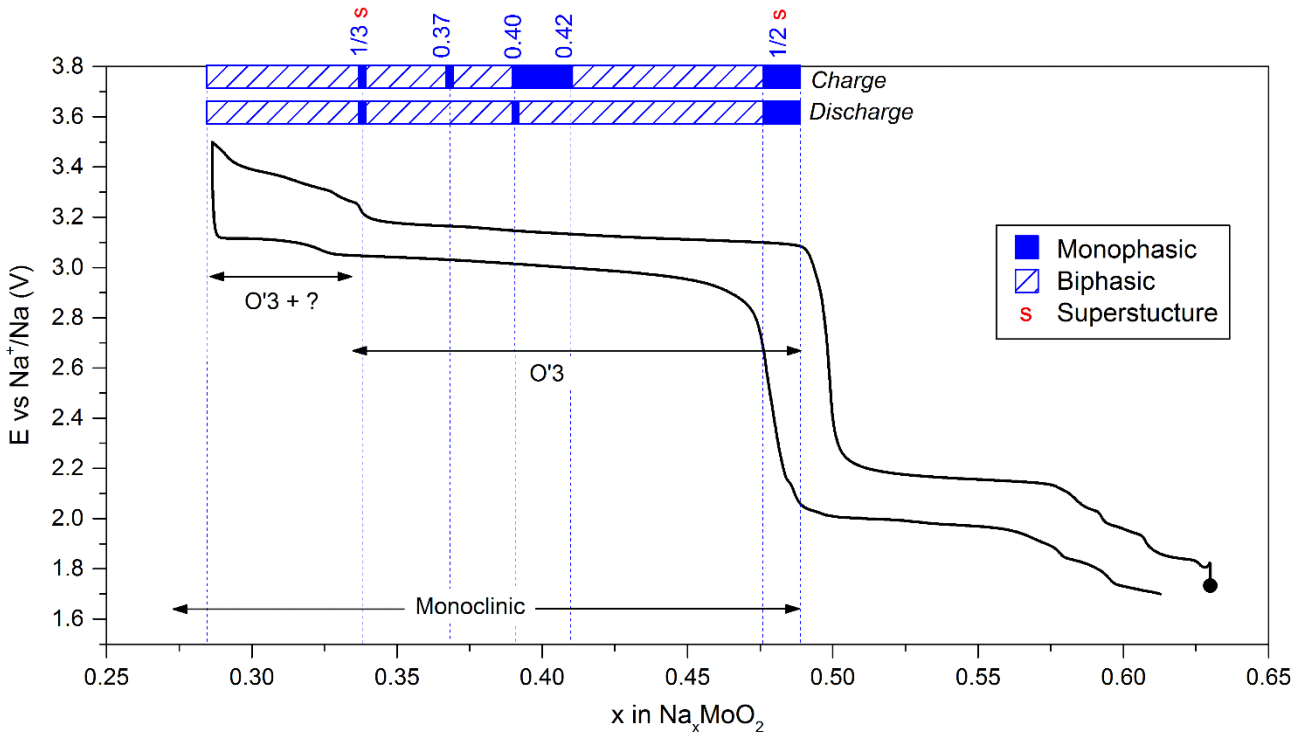

Figure 8: Correlation between the variations observed on the electrochemical curve and the phase diagram determined by in sit u X-ray diffraction. A complete phase diagram for the composition range is presented on the top. Monophasic domains and biphasic domains are stated respectively by blue and striped areas. Sodium contents of each specific phases are written in blue. Superstructures are highlighted by a red ≪ s ≫. Structure types are also reported on the electrochemical curve.

On the contrary, in the composition range $0.5 \leq x \leq 1$, $(MoO_2)_n$ layers were found to reversibly glide during the electrochemical process to give rise to trigonal prismatic sites for sodium ions for Na_xMoO_2 phases within the composition range $0.58 \leq x \leq 0.72$.[13]

On the peculiar behavior of the 0.50 -0.37 domain.

From a general point of view, upon ionic de-intercalation the average in-plane metal-metal distance monotonously decreases while the interslab distance increases in layered oxides.[29] This is observed in the Na_xMoO_2 system in the composition range $0.5 < x < 1$.[13] For $x < 0.5$ the opposite effect is observed: in-plane metal-metal average distance which corresponds to the b-parameter increases and the interslab distance decreases (Table I). This anomalous increase of the in-plane distance upon oxidation could result from a decrease of the number of Mo-Mo bonds in the $(MoO_2)_n$ layers when Mo^{3+} (d^3) is oxidized to Mo^{4+} (d^2).

The peculiar behavior observed in the 0.5 - 0.37 domain leads to the following question: are these solid solutions or biphasic domains? Both end members ($x = 0.37$ and $x = 0.50$) are quite well crystalized with well-defined diffraction reflections. Some diffraction reflections do not exhibit broadening while some other are strongly modified. This behavior is characteristic of the formation of stacking faults in the stacking of the $(MO_2)_n$ layers. As discussed in the previous part, sodium ions stay in octahedral interstitial sites. Therefore, one can assume that the defects result from the distribution of Mo ions within the $(MoO_2)_n$ slabs. If the two phases present different Mo patterns due to different Mo-Mo bonding, the nucleation of one phase into the other does not occur in a statistical way, which would not lead to a true solid solution, but to the formation of small domains leading to the appearance of pseudo-phases on the X-ray diffraction pattern (Figure 6).

From the electrochemical point of view, an average potential is observed suggesting a solid solution behavior. The classical electrochemical model used to describe the behavior of battery materials is valid only for ideal structures. A similar behavior was observed for the alpha/gamma transition occurring in cycling of the Nickel electrode on the Ni-Cd batteries but not explained at that time.[30]

Conclusions

We have shown that the electrochemical sodium (de)intercalation in the Na_xMoO_2 material is reversible in the $0.25 \leq x \leq 0.63$ composition range. The phase diagram of the Na_xMoO_2 system for low sodium contents ($x \leq 0.5$) has been established by *in situ* X-ray diffraction. **Figure 8** resumes the phase diagram during the charge and the discharge of a battery made of $Na_{2/3}MoO_2$ at the positive electrode and it shows a good agreement between the structural transitions evidenced by *in situ* X-ray diffraction and the voltage variation on the electrochemical curve. The phase diagram is less complex than the one previously determined for sodium contents $x \geq 0.5$,[13] but three single phase domains ($0.4 \leq x \leq 0.42$, $x = 0.37$ and $x = 0.33$) have still been evidenced during the charge. Furthermore, X-ray diffraction patterns for the $Na_{0.5}MoO_2$ and $Na_{0.33}MoO_2$ phases are characterized by the presence of superstructure peaks suggesting the existence of specific atomic arrangements

in the structure. This could result from sodium/vacancy orderings and/or from the patterning of Mo-Mo bonds within the $(MoO_2)_n$ slabs, which was confirmed by pair distribution functions analysis in the $Na_{0.5}MoO_2$ phase. The occurrence of these Mo-Mo interactions could modify the transport properties of the positive electrode material during cycling, making the use of molybdenum sodium layered oxides in real sodium-ion batteries unlikely. The existence of a highly deintercalated Na_tMoO_2 phase has been evidenced at high voltage.

Conflicts of interest

There are no conflicts to declare.

Acknowledgements

MG would like to thank the Agence Nationale de la Recherche for providing support through the grant ANR-14-CE05-0011. This research used resources of the Advanced Photon Source, a U.S. Department of Energy (DOE) Office of Science User Facility operated for the DOE Office of Science by Argonne National Laboratory under Contract No. DE-AC02-06CH11357. MG would like to thank Olag Borkiewicz from the Advanced Photon Source for collecting the pair distribution functions data. MG and CD would like to thank Bertrand Guillaume from the ICMCB for building the electrochemical cell which was used for the *in situ* experiment.

Notes and references

1 M. S. Goldsztaub, *C. R. Acad. Sc. Paris*, 1933, **196**, 280; W. Rüdorff and H. Becker, *Z. Naturforschg. B*, 1954, **9**, 614; L. D. Dyer, B. S. Bori, and J. P. Smith., *J. Am. Chem. Soc.*, 1954, *76*, 1499; M. Dodero and C. Déportes, *C. R. Acad. Sc. Paris*, 1956, **242**, 2939; P. Hagenmuller, A. Lecerf and M. Onillon, *C. R. Acad. Sc. Paris*, 1962, **255**, 928; R. Scholder and U. Protzer, *Z. Anorg. Allg. Chem.*, 1969, **369**, 313.

2 J. P. Parent, R. Olazcuaga, C. Devalette, M. and Fouassier and P. Hagenmuller, *J. Solid State Chem.,* 1971, **3**, 1; C. Fouassier, G. Matejka, J. M. Réau and P Hagenmuller, *J. Solid State Chem.*, 1973, **6**, 532.

3 C. Delmas, J.-J. Braconnier, C. Fouassier and P. Hagenmuller, *Solid State Ion.*, 1981, **3-4**, 165; J.-J. Braconnier, C. Delmas and P. Hagenmuller, *Mater. Res. Bull.*, 1992, **17**, 993; A. Mendiboure, C. Delmas and P. Hagenmuller, *J. Solid State Chem.*, 1985, **57**, 323.

4 V. Palomares, M. Casas-Cabanas, E. Castillo-Martinez, M. H. Han and T. Rojo, *Energy Environ. Sci.*, 2013, **6**, 2312; K. Kubota and S. Komaba, *J. Electrochem. Soc.*, 2015, **162**, A2538; J.-Y. Hwang, S.-T. Myung and Y.-K. Sun, *Chem. Soc. Rev.*, 2017, **46**, 3529; C. Delmas, *Adv. Energy Mater.*, 2018, **8**, 1703137.

5 M. Roger, D. J. P. Morris, D. A. Tennant, M. J. Gutmann, J. P. Goff, J.-U. Hoffmann, R. Feyerherm, E. Dudzik, D. Prabhakaran, A. T. Boothroyd, N. Shannon, B. Lake, P. P. Deen, *Nature*, 2007, **445**, 631.

6 Y. Wang, R. Xiao, Y.-S. Hu, M. Avdeev and L. Chen, *Nat. Commun.*, 2015, 6, 6954; X. Li, D. Wu, Y.-N. Zhou, L. Liu, X.-Q. Yang and G. Ceder, *Electrochem. Commun.,* 2014, **49**, 51.

7 S. Komaba, T. Nakayama, A. Ogata, T. Shimizu, C. Takei, S. Takada, A. Hokura, I. Nakai, *ECS Trans.*, 2009, **16**, 43; C. Didier, M. Guignard, C. Denage, O. Szajwaj, S. Ito, I. Saadoune, J. Darriet, C. Delmas, *Electrochem. Solid-State Lett.* 2011, **14**, A75; D. Hamani, M. Ati, J.-M. Tarascon, P. Rozier, *Electrochem. Commun.*, 2011, **13**, 938; N. Yabuuchi, H. Yoshida and S. Komaba, *Electrochemistry*, 2012, **80**, 716; P. Vassilaras, X. Ma, X. Li and G. Ceder, *J. Electrochem. Soc.*, 2013, **160**, A207; M. Guignard, C. Didier, J. Darriet, P. Bordet, E. Elkaïm, and C. Delmas, *Nat. Mater.*, 2013, **12**, 74; M. H. Han, E. Gonzalo, M. Casas-Cabanas, T. Rojo, *J. Power Sources*, 2014, **258**, 266.

8 Q. Huang, M. L. Foo, J. W. Lynn, H. W. Zandbergen, G. Lawes, Y. Wang, B. H. Toby, A. P. Ramirez, N. P. Ong and R. J. Cava, *J. Phys. : Condens. Matter*, 2004, **16**, 5803

9 M. Guignard and C. Delmas, *ChemistrySelect*, 2017, **2**, 5800.

10 A. Maazaz, C. Delmas and P. Hagenmuller, *J. Incl. Phenom.*, 1983, **1**, 45 ; Y. Takeda, K. Nakahara, M. Nishijima, N. Imanishi, O. Yamamoto, M. Takano and R. Kanno, *Mater. Res. Bull.*, 1994, **29**, 659.

11 J.-M. Tarascon, G. W. Hull, *Solid State Ion.*, 1986, **22**, 85.

12 A. Mendiboure, H. Eickenbusch, R. Schöllhorn, G.V. Subba Rao, *J. Solid State Chem.*, 1987, **71**, 19; S.-H. Chang, H.-H. Park, A. Maazaz, C. Delmas, *C. R. Acad. Sc. Paris*, 1989, **308**, 475.

13 L. Vitoux, M. Guignard, M. R. Suchomel, J. C. Pramudita, N. Sharma and C. Delmas, *Chem. Mater.*, 2017, **29**, 7243.

14 J.-M. Reau, C. Fouassier and P. Hagenmuller, P. *Bull. Société Chim. Fr.* 1970, **11**, 3827.

15 V. Petricek, M. Dusek and L. Palatinus, *Z. Krist.-Cryst. Mater.*, 2014, **229**, 345.

16 P. Juhas, T. Davis, C. L. Farrow and S. J. L. Billinge, *J. Appl. Cryst.,* 2013, **46**, 560.

17 C. L. Farrow, P. Juhas, J. W. Liu, D. Bryndin, E. S. Bozin, J. Bloch, T. Proffen, S. J. L. Billinge, *J. Phys.: Condens. Matter,* 2007, **19**, 335219.

18 A. Ponrouch, E. Marchante, M. Courty, J.-M. Tarascon and M. R. Palacin, *Energy Environ. Sci.*, 2012, **5**, 8572.

19 R.E. McCarley, K.-H. Lii, P.A. Edwards and L.F. Brough, *J. Solid State Chem.*, 1985, **57**, 17.

20 S. Levasseur, M. Ménétrier, E. Suard and C. Delmas, *Solid State Ion.*, 2000, **128**, 11; S. Levasseur, M. Ménétrier, Y. Shao-Horn, L. Gautier, A. Audemer, G. Demazeau, A. Largeteau and C. Delmas, *Chem. Mater.*, 2003, **15**, 348.

21 R. Berthelot, D. Carlier, C. Delmas, *Nat. Mater.*, 2011, **10**, 74.

22 Y. Wang, Y. Ding and J. Ni, *J. Phys.: Condens. Matter*, 2009, **21**, 035401 ; A. J. Toumar, S. P. Ong, W. D. Richards, S. Dacek and G. Ceder, Phys. Rev. Applied, 2015, 4, 064002.

23 B. Mortemard de Boisse, D. Carlier, M. Guignard, L. Bourgeois and C. Delmas, C. *Inorg. Chem.,* 2014, **53**, 11197; B. Mortemard de Boisse, J.-H. Cheng, D. Carlier, M. Guignard, C.-J. Pan, S. Bordère, D. Filimonov, C. Drathen, E. Suard, B.-J. Hwang, A. Wattiaux and C. Delmas, C. *J Mater Chem A,* 2015, **3**, 10976.

24 Z. Lu and J. R. Dahn, *J. Electrochem. Soc.*, 2001, **148**, A1225.

25 L. Croguennec, C. Pouillerie, A. N. Mansour and C. Delmas, *J. Mater. Chem.,* 2001, **11**, 131.

26 L. Seguin, G. Amatucci, M. Anne, Y. Chabre, P. Strobel, J.-M. Tarascon and G. Vaughan, *J. Power Sources,* 1999, **81–82**, 604.

27 G. G. Amatucci, J.-M. Tarascon, L. C. Klein, *J. Electrochem. Soc.*, 1996, **143**, 1114.

28 C. Louchet-Pouillerie, PhD Thesis, Université Bordeaux 1, 2000.

29 C. Pouillerie, L. Croguennec and C. Delmas, *Solid State Ion.*, 2000, **132**, 15.

30 P. Oliva, J. Leonardi, J.-F. Laurent, C. Delmas, J.-J. Braconnier, M. Filgarz, F. Fievet and A. de Guibert, *J. Power Sources*, 1982, **8**, 229.